Defects in irradiated silicon: EPR and electron-nuclear double resonance of interstitial boron

G. D. Watkins*

General Electric Corporate Research and Development, Schenectady, New York 12301
(Received 15 May 1975)

An EPR spectrum, labeled Si-$G28$, is identified as arising from neutral interstitial boron in silicon. It is produced by 1.5-MeV electron irradiation at 20.4 °K, presumably when a substitutional boron atom traps a mobile interstitial silicon atom which is produced in the original damage event. Three possible models are discussed which are consistent with the EPR and electron-nuclear double-resonance results: (a) a bent Si-B-Si bonded interstitialcy; (b) a similar Si-Si-B interstitialcy; or (c) a Jahn-Teller distortion of the boron from the hexagonal interstitial site in the silicon lattice. Uniaxial stress in the presence of light at low temperatures produces alignment in one of the distortional degrees of freedom for the defect. This is interpreted as stress alteration of the capture matrix elements for electrons into the differently distorted configurations. Polarized light is also found to produce alignment in the absence of stress into a second degree of freedom for the defect. Thermally activated recovery from this alignment reveals an activation energy for reorientation of 0.6 eV. Interstitial boron is unstable at room temperature, disappearing in ~ 30 min with an activation energy also of ~ 0.6 eV. It is suggested that annealing may result from long-range migration of the interstitial boron with the one-jump diffusional process being identical to the 0.6-eV reorientational process. This is a natural consequence of models (a) or (c). The reorientation stimulated by light at 4.2 °K, therefore, indicates that athermal migration may be induced by the light. An attempt to test this using 1.06-μm YAlG:Nd laser illumination was inconclusive.

I. INTRODUCTION

We have previously reported the formation of interstitial aluminum in silicon by 1.5-MeV electron irradiation at 20.4 and 4.2 °K.[1-3] Interstitial aluminum was found to be a double donor and, in the Al^{++} state, careful EPR[1,4] and electron-nuclear double-resonance (ENDOR)[4] studies revealed that it resides in the symmetrical tetrahedral (T_d) interstitial site.

The mechanism of formation was suggested to be the replacement of a substitutional aluminum atom by an interstitial silicon atom, which was produced in the initial damage event and is mobile at the irradiation temperature.[1] This model has served as the basis from which all present models of the role of the interstitial in radiation damage of silicon derive.

The dominant p-type dopant in commercial silicon devices is not aluminum but is boron. Most studies of the electrical and optical properties of irradiated p-type silicon have, therefore, been in boron-doped silicon. Attempts to interpret the results have had for the most part to rely upon the understanding derived from the EPR studies in aluminum-doped material.

In this paper we attempt to rectify this situation. We report a detailed study of interstitial boron observed via its electron paramagnetic resonance spectrum, labeled Si-G28. We confirm that the same interstitial trapping occurs at low temperatures in boron-doped material. Unlike Al^{++}, however, the boron is not in the normal tetrahedral site. Its electrical activity is also different, being

both a single donor and acceptor. It is also less stable, annealing at room temperature.

II. EXPERIMENTAL PROCEDURE

Most of the experimental techniques relevant to these studies have been described in previous publications.[5,6] EPR studies were performed at ~ 20 GHz and observed primarily at 20.4 °K in dispersion. ENDOR was performed at 4.2 °K. Most of the samples studied were boron-doped ($\sim 10^{16}$ cm^{-3}) vacuum floating-zone silicon obtained from commerical sources. They were irradiated *in situ* at 20.4 °K with 1.5-MeV electrons from a resonant transformer accelerator.

Light was introduced to the sample via a fused quartz light pipe from outside the cryostat. Polarization was achieved by an HR-2 polaroid filter on the end of the pipe just above the sample.

III. EXPERIMENTAL RESULTS AND DISCUSSION

A. Experimental results

1. General

The Si-G28 spectrum observed at 20.4 °K is shown in Fig. 1. It is produced by 1.5-MeV electron irradiation at ~ 20.4 °K and only in boron-doped silicon. It has been observed in both vacuum floating zone (oxygen $\lesssim 10^{16}$ cm^{-3}) and pulled (oxygen $\sim 10^{18}$ cm^{-3}) p-type crystals. In both materials the production rate is high, being roughly comparable to that for single-vacancy (V) production as monitored by the V^+ spectrum.[1,7] It has also been observed in n-type silicon partially
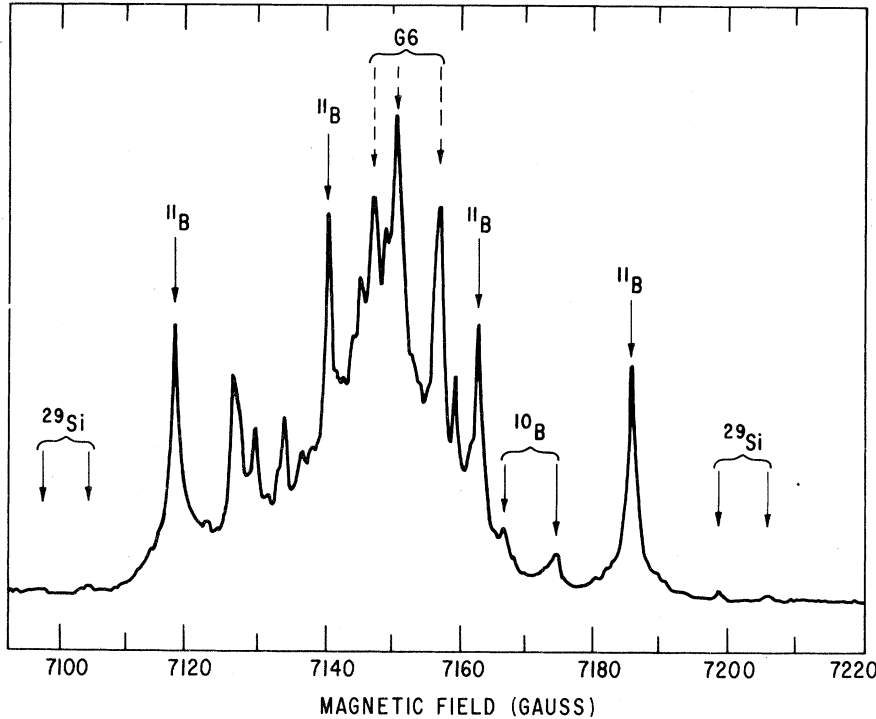
FIG. 1.   Si-G28 spectrum at 20.4°K, $\vec{H} \parallel \langle 111 \rangle$, $\nu_0 = 20.0$ GHz. Some of the resolved hyperfine multiplets are indicated.

counterdoped with boron. (In this material the low-temperature production rate was an order of magnitude less, as was the single-vacancy production.[7])

The charge state of the defect giving rise to the Si-G28 spectrum does not appear to be stable in either low resistivity n- or p-type material at 20.4°K. In each case, near-band-gap light is required to generate the spectrum. In low-resistivity material, the spectrum decays when the light is turned off. In p-type silicon, made high resistivity after prolonged irradiation, the Si-G28 spectrum, once generated by light, remains indefinitely at 20.4°K. Warming to ~50°K in the dark removes the spectrum.

2. EPR and ENDOR spectra

The angular dependence of the spectrum is complex and can be resolved unambiguously only for the outermost groups of lines, as shown in Fig. 2(a). This is sufficient, however, for analysis. The spectrum is analyzed as arising from a single anisotropic defect species, but distributed among the various defect orientations within the lattice, and described by the spin Hamiltonian.

$$\mathcal{H} = \mu_B \vec{H} \cdot \vec{g} \cdot \vec{S} + \sum_j \{ \vec{I}_j \cdot [\vec{A}_j \cdot \vec{S} - (\mu_j / I_j) \vec{H}]$$

$$+ \vec{I}_j \cdot \vec{Q}'_j \cdot \vec{I}_j \}, \tag{1}$$

with $S = \frac{1}{2}$.

Well-resolved hyperfine interactions with the nuclei of three distinct atoms j near the defect are observed. One is with a single boron atom, as evidenced by the $2I_j + 1 = 4$ multiplets in Fig. 1 arising from ^{11}B (81% abundant, $I = \frac{3}{2}$). Weaker multiplets arising from ^{10}B (19% abundant, $I = 3$) can also be seen. Two pairs of weak satellites can also be seen in the wings of the spectrum. These arise from hyperfine interaction with ^{29}Si (4.7% abundant, $I = \frac{1}{2}$) at two nonequivalent neighboring silicon atom sites.

The results of analysis are summarized in Fig. 3 for one of the equivalent defect orientations in the lattice. The g values and ^{29}Si hyperfine interactions were determined directly from the EPR spectrum. The g values were estimated from the center of gravity of the extreme ^{11}B hyperfine multiplets ($m = \pm \frac{3}{2}$), and their angular dependence is shown in Fig. 2(b). The ^{29}Si hyperfine tensors were estimated from the angular dependence of the displacements of the resolved satellites from the corresponding ^{11}B hyperfine $m = \pm \frac{3}{2}$ multiplet.

The ^{11}B hyperfine parameters were determined from ENDOR studies. Here ENDOR transitions were studied versus magnetic field orientation for most of the resolved ^{11}B hyperfine multiplets in the EPR spectrum. The method of analysis has been described in detail previously[8] and will not be repeated here. Briefly, the principal axes of $\vec{A}$ and $\vec{Q}'$ were determined from the extrema versus orientation of $\vec{H}$ of the sums and differences, re-
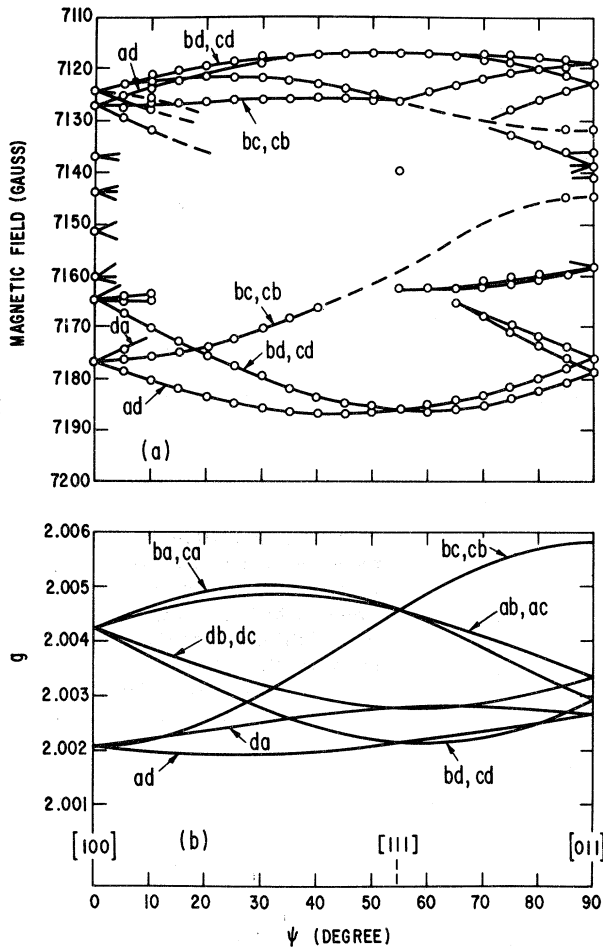
FIG. 2. (a) Angular dependence of the resolved structure, with $\vec{H}$ in the $(01\bar{1})$ plane, see Fig. 3. (b) Angular dependence of g.

spectively, of the nuclear transitions associated with the $M = +\frac{1}{2}$ and $M = -\frac{1}{2}$ electronic Zeeman states. [Anisotropy in $\vec{A}$ causes the effective field at the nucleus to depart from the direction of $\vec{H}$ when it is not along a principal axis of $\vec{A}$. This must be corrected for in determining the principal axes of $\vec{Q}'$ (see Ref. 13 in Ref. 8). For instance, the $10°$ difference between the A_1 and Q_1' axes given in Fig. 3 is observed as a $25°$ difference in the external field $\vec{H}$ direction.] The principal values of $\vec{A}$ and $\vec{Q}'$ were determined by analysis of the transitions with $\vec{H}$ along the three principal axes of $\vec{A}$. Solution of Eq. (1) to first order in $Q'/$ $|MA - (\mu/I)H|$ and second order in $A/g\mu_B H$ was found to be sufficient. The absoulte signs of the components of $\vec{A}$ and $\vec{Q}'$ could not be determined, but their relative signs, indicated by the choice of either the upper or lower sign throughout Fig. 3, were.

For later use, we label the transitions of Fig. 2 as referring to specific defect orientations. In Fig. 3 the four $\langle 111 \rangle$ axes are labeled a, b, c, and d. We label a defect orientation by two letters. The first letter denotes the $\langle 111 \rangle$ axis closest to g_3 (or A_3, Q_3), the second, the $\langle 111 \rangle$ axis closest to g_1 (or A_1, Q_1). The defect orientation illustrated in Fig. 3 is, therefore, cb.

3. Analysis of the magnetic hyperfine interactions

Following the procedure used for the analysis of previous centers,[6,8] we approximate the wave function for the unpaired electron by a linear combination of atomic orbitals centered on the atoms near the defect:

$$\Psi = \sum_j \eta_j \psi_j \ . \tag{2}$$

At each site j we approximate ψ_j as a hybrid ns-np orbital:

$$\psi_j = \alpha_j (\psi_{ns})_j + \beta_j (\psi_{np})_j \ , \tag{3}$$

where $n = 3$ for Si and $n = 2$ for B. To a good first approximation, the magnetic hyperfine interaction at the jth nuclear site is determined solely by ψ_j, i.e., that part of the wave function close to the nucleus. This leads to a hyperfine tensor with axial symmetry around the p-function axis,

$$(A_{\parallel})_j = a_j + 2b_j \ ,$$
$$(A_{\perp})_j = a_j - b_j \ . \tag{4}$$

Here

$$a_j = \tfrac{16}{3}\pi(\mu_j/I_j)\,\mu_B \alpha_j^2 \eta_j^2 |\psi_{ns}(0)|_j^2 \tag{5}$$

and

$$b_j = \tfrac{4}{5}(\mu_j/I_j)\mu_B \beta_j^2 \eta_j^2 \langle r_{np}^{-3} \rangle_j \ , \tag{6}$$

where μ_B is the Bohr magneton, μ_j is the magnetic moment, and I_j the spin of the jth nucleus.

For boron, the value of $\langle r_{2p}^{-3} \rangle$ was obtained from experimental atomic beam hyperfine measurements for the neutral atom.[9] An estimate of $|\psi_{2s}(0)|^2$ was obtained by scaling the above value for $\langle r_{2p}^{-3}\rangle$ by the ratio $|\psi_{2s}(0)|^2/\langle r_{2p}^{-3} \rangle$ calculated from Hartree wave functions.[10,11] This procedure has been described elsewhere[6] where corresponding values for silicon have been estimated. The results are

boron: $\quad |\psi_{2s}^2(0)| = 9.86(10^{24})$ cm^{-3} ,

$\qquad\qquad \langle r_{2p}^{-3} \rangle = 5.42(10^{24})$ cm^{-3} ;

silicon: $\quad |\psi_{3s}^2(0)| = 31.5(10^{24})$ cm^{-3} ,

$\qquad\qquad \langle r_{3p}^{-3} \rangle = 16.1(10^{24})$ cm^{-3} .

Using these values, we can solve Eqs. (5) and (6) for α_j^2, β_j^2 and η_j^2, using the hyperfine constants given in Fig. 3. The results are given in Table I. The signs indicated for a_j and b_j reflect that of μ_j as expected from Eqs. (5) and (6). They are enclosed in parentheses to indicate that they
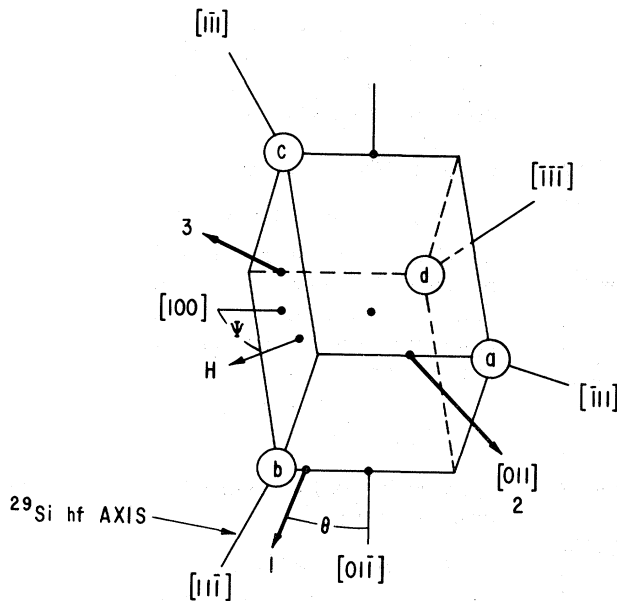
FIG. 3. Spin-Hamiltonian constants and relevant axes for one of the twelve defect orientations in the lattice. With the magnetic field $\vec{H}$ in the $(01\bar{1})$ plane as shown, this set of axes corresponds to the defect labeled cb.

$g_1 = 2.0019 \pm 0.0001$

$g_2 = 2.0058 \pm 0.0001$

$g_3 = 2.0028 \pm 0.0001$

$\theta = 65 \pm 7°$

$^{29}\text{Si} \begin{cases} A_\parallel(1) = 37.5 \pm 1.0 \ (10^{-4}\text{cm}^{-1}) \\ A_\perp(1) = 24.3 \pm 3.0 \ (10^{-4}\text{cm}^{-1}) \\ \\ A_\parallel(2) = 19.0 \pm 1.0 \ (10^{-4}\text{cm}^{-1}) \\ A_\perp(2) = 0 \pm 5.0 \ (10^{-4}\text{cm}^{-1}) \end{cases}$

$\theta^{\text{I}} \sim \theta^{\text{II}} \sim 35.3°$

$^{11}\text{B} \begin{cases} A_1 = \pm 21.512 \pm 0.003 \ (10^{-4}\text{cm}^{-1}) \\ A_2 = \pm 4.103 \pm 0.006 \ (10^{-4}\text{cm}^{-1}) \\ A_3 = \pm 4.213 \pm 0.006 \ (10^{-4}\text{cm}^{-1}) \\ \qquad\quad \theta = 42.4 \pm 0.4° \\ \\ Q'_1 = \pm 0.033 \pm 0.001 \ (10^{-4}\text{cm}^{-1}) \\ Q'_2 = \pm 0.023 \pm 0.002 \ (10^{-4}\text{cm}^{-1}) \\ Q'_3 = \mp 0.056 \pm 0.002 \ (10^{-4}\text{cm}^{-1}) \\ \qquad\quad \theta = 52 \pm 3° \end{cases}$

were not determined experimentally.

From Table I we conclude that ~33% of the wave function is located in a p orbital on a single boron atom. An equal amount is shared between two nearby silicon atoms. In this way 67% of the wave function is accounted for, a value similar to that generally found in such an analysis for other radiation-produced defects in silicon.[5,6,8,12-14]

4. Analysis of the quadrupole interaction

The quadrupole constant Q'_j along a principal axis i is given by[15]

$$Q'_i = e^2 q_i \, Q / 2I(2I-1) \,, \tag{7}$$

where eQ is the nuclear electric quadrupole mo-

ment and eq_i is the electric field gradient along this axis at the nucleus. Since the magnitude of eq at the nucleus receives its greatest contribution from the lowest partially filled p orbitals,[16] Q'_i can be conveniently related to the degree of unbalanced charge density in the $2p$ orbitals of the boron atom. The ^{11}B quadrupole coupling constant for an electron in a single $2p$ orbital directed along axis i (i.e., $m_i = 0$) can be estimated from the coupling constant measured from atomic beam studies[9]

$$(e^2 q_i \, Q)_{pi} = -2(e^2 qQ)_{\text{atom}} = -1.798(10^{-4}) \text{ cm}^{-1} \,.$$

The measured values of Q'_i, Fig. 3, therefore, indicate an unbalanced charge density equivalent

TABLE I. Hyperfine parameters (a_j and b_j) and the corresponding molecular wave-function coefficients (α_j^2, β_j^2, and η_j^2) calculated from the observed hyperfine-interaction constants.

Atom	a_j (10^{-4} cm^{-1})	b_j (10^{-4} cm^{-1})	α_j^2	β_j^2	η_j^2
^{11}B	(+) 7.74	(+) 5.79	0.03	0.97	0.33
^{29}Si(1)	(−) 28.7	(−) 4.4	0.14	0.86	0.15
^{29}Si(2)	(−) 6.3	(−) 6.3	0.02	0.98	0.19

to ~19% that of a pure $2p$ orbital directed along the three axis. (We ignore the small anisotropy from axial symmetry of $\vec{Q}'$.) The sign of Q_3', arrived at assuming A_j positive, indicates an excess electronic charge density along the three axis.

B. Discussion

1. General

Previous studies in aluminum-doped p-type silicon[1-3] have demonstrated that the principal defects produced by 1.5-MeV electron irradiation at $\gtrsim 20.4$ °K are isolated lattice vacancies and interstitial Al^{++} ions. This has been interpreted to indicate that the interstitial silicon atom, produced in the primary damage event, is mobile at this low temperature and is trapped by the substitutional group-III atom, producing interstitial aluminum.[1]

In the boron-doped material studied here the isolated vacancy is observed to be produced at essentially the same rate as in the corresponding aluminum-doped material. The only significant difference is the formation of the Si-G28 spectrum instead of that of interstitial Al^{++}. The resolved ^{11}B hyperfine interaction demonstrates unambiguously the presence of a boron atom in the defect.

We, therefore, conclude that the Si-G28 spectrum arises from interstitial boron. The low symmetry of the spectrum reveals, however, that the boron is not situated in the center of the normal tetrahedral (T_d) or hexagonal (D_{3d}) interstitial site. Rather it must be distorted out of such a position, perhaps into a bonded "interstitialcy"-like configuration. This contrasts with interstitial Al^{++} which was observed to have the full T_d symmetry of the undistorted tetrahedral interstitial site.[1,4]

2. Model

In Fig. 4(a) we suggest a possible model for the defect. Here a neutral boron atom is nestled into a bonded configuration between two normal nearest-neighbor silicon atoms. It is not in line with the nearest-neighbor silicon atoms but forms a bent-bond structure as shown. Such a configuration is perhaps not unreasonable, being similar to that established for interstitial oxygen,[17-19] which comes from the same row in the periodic table. In this model the Q_3' axis reflects the ex-
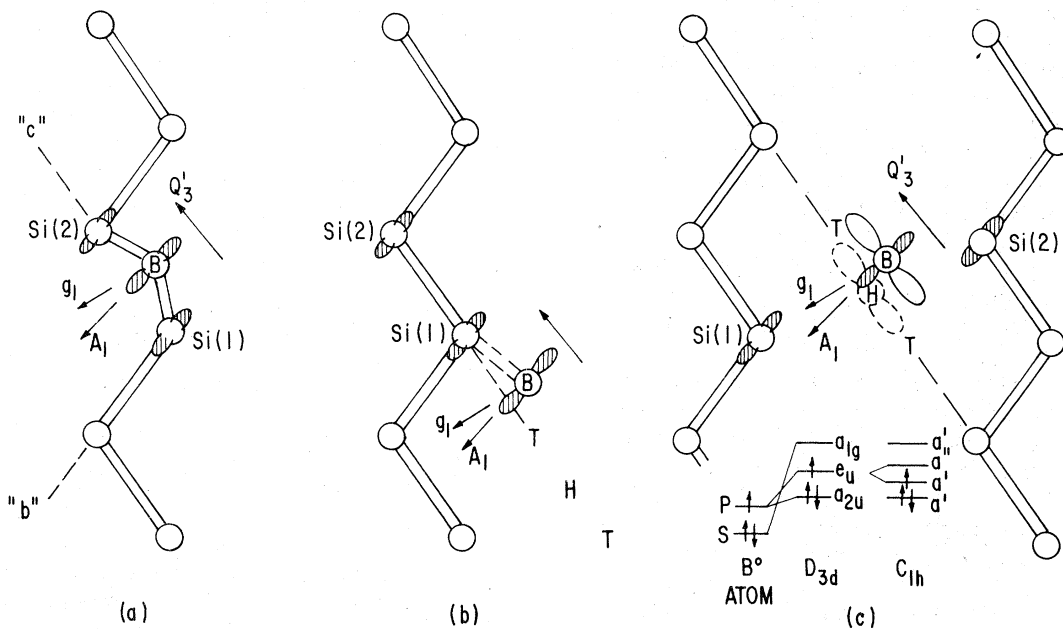

FIG. 4. Models for neutral interstitial boron: (a) a bent-bond Si-B-Si interstitialcy; (b) a bent-bond Si-Si-B configuration, which can be viewed as a distortion from the tetrahedral interstitial site (T); (c) a Jahn-Teller distortion from the hexagonal interstitial site (H). In (c) the Jann-Teller distortion arises from the degeneracy of the e_u orbital ($D_{3d} \rightarrow C_{1h}$) and does not exist for B$^+$.

cess electronic charge density associated with the Si-B-Si bonding. The hyperfine (A_1) and g-tensor (g_1) axes on the other hand reflect the unpaired electron orbital which, on the boron atom, is comprised of a nonbonding p orbital, directed as shown. In this bent configuration, the two neighbor atoms, Si(1) and Si(2), are inequivalent and are identified as the two inequivalent silicon atoms observed in the resolved hyperfine interactions, as shown.

A second model is considered in Fig. 4(b). This can be viewed as a simple displacement of the boron atom from the T_d interstitial position, as shown. If the boron atom were to retain its ground sp^2 configuration, the distortion could be viewed simply as a Jahn-Teller effect, associated with the degeneracy of the singly occupied p orbital. However, in this case the quadrupole interaction would be expected to reflect this p orbital and have its major axis parallel to A_1. The configuration of Fig. 4(b) would, therefore, appear to be consistent with the observed quadrupole interaction only if the boron entered into substantial bonding with Si(1) and its filled orbitals had substantial p character along the B-Si(1) direction. As such, both models of Figs. 4(a) and 4(b) can be viewed as distorted $\langle 111 \rangle$ bonded interstitialcy configurations, that of Fig. 4(a) being (Si-B-Si), that of Fig. 4(b) being (Si-Si-B).

A third model is considered in Fig. 4(c). This can be viewed as a simple displacement of the boron atom from the hexagonal interstitial position (H), as shown. This represents a nonbonding position for the boron atom, the Q_3' axis here reflecting a filled nonbonding atomic p orbital directed along the open interstitial channel. A simple molecular orbital model for this structure is also included in the figure. In this model the cage of silicon atoms surrounding an interstitial site is considered to be strongly repulsive to the boron electronic orbitals because all of the silicon bonding states are filled. This inverts the normal s-p energy splitting for the free boron atom, the more compact p orbitals now being lower in energy. In the hexagonal site (D_{3d}) the a_{2u} orbital is the p state directed in the $\langle 111 \rangle$ direction along the open interstitial space (perpendicular to the plane of the puckered six-membered ring of silicon atoms surrounding the hexagonal site), and is lowest in energy because it overlaps least with the silicon atom bonding electron density. In the B^+ state, two electrons are in this p orbital and the hexagonal site would be the stable position. For B^0, the third electron goes into an e_u orbital (p function in the plane of the Si_6 ring) and a Jahn-Teller distortion results.

In this third model, ^{29}Si hyperfine interactions would arise from admixtures of the corresponding

symmetry orbitals on the surrounding silicon atoms. For the six atoms in the puckered ring surrounding the hexagonal (D_{3d}) site, both overlap and symmetry (e_{1u}) considerations suggest dominant contributions from the pair which are approximately in line with the unpaired orbital p function on the boron, i.e., the pair in the plane of Fig. 4(c) as indicated. The distortion from the hexagonal site would destroy their equivalence, consistent with the observation of two inequivalent hyperfine interactions.

Of the three models, the Si-B-Si interstitialcy of Fig. 4(a) is, in many respects, the logical choice. As has already been mentioned, oxygen, from the same row in the periodic table, is known to enter into such a bonding configuration in silicon. The quadrupole and hyperfine parameters appear to follow logically from the model. In addition, calculations using extended Huckel theory (EHT) on large clusters of carbon atoms have predicted that the boron interstitial prefers a bonded interstitialcy configuration in the similar material, diamond.[20]

However, in Sec. VI, it will be found that one experimental result is difficult to reconcile with the model of Fig. 4(a). As a result, the models of Figs. 4(b) and 4(c) must be considered realistic candidates. In this regard, the EHT calculations of interstitials in diamond did indicate a reversal of the s-p atomic splitting with the p-orbital energy lowest in the hexagonal and tetrahedral sites.[20] This requirement, common to some extent for the models of both Figs. 4(b) and 4(c) (in order to explain the p-orbital charge density revealed by Q_3'), therefore receives some justification from these calculations.

The configurations and axes shown for the models of Fig. 4 are drawn to correspond to the axes of Fig. 3 and, therefore, correspond to the defect labeled cb. We note that the first label defines the preferential $\langle 111 \rangle$ axis as revealed by Q_3'. The second letter defines the direction of the off-axis distortion of the boron as revealed by A_1 and g_1.

IV. MOTIONAL EFFECTS

A. Low-temperature stress studies

In p-type silicon made high resistivity after prolonged irradiation, the Si-G28 spectrum was first generated with light and then the light was turned off. In such high-resistivity material, the Si-G28 spectrum remains indefinitely at 4.2 or 20.4 °K and can be studied in the absence of light. Uniaxial stress up to ~ 500 kg/cm^2 was then applied along a $\langle 110 \rangle$ axis of the crystal. No change was detected in the relative intensities of any of the spectral components at either 4.2 or 20.4 °K. Also, no change was detected as the sample was

allowed to warm to ~50 °K with stress applied, at which point the spectrum disappears. We conclude, therefore, that the defect cannot reorient as a result of thermal activation at these temperatures.

The sample was also cooled under stress from $T \gtrsim 180$ to 20.4 °K. The stress was then removed and the signal generated by light. Again, no detectable alignment of the defects was detected.

However, if stress is applied at 4.2 or 20.4 °K *in the presence of light*, significant alignment is observed. If the light is then turned on in the absence of stress, the alignment is removed. The rate of the buildup or decay of the alignment is proportional to the intensity of illumination and appears to be equal to the initial generation rate of the spectrum.

If the defects are aligned and then warmed with both stress and light removed, the alignment remains until ~50 °K at which point the spectrum is lost. Upon recooling to 20.4 °K and regeneration with light, the spectrum reemerges but with the alignment gone. Alternatively, if the spectrum is regenerated with the stress on, it emerges with full alignment. Prolonged illumination with stress does not increase the degree of alignment.

We conclude, therefore, that the alignment is achieved during the electron-capture process that produces the Si-G28 charge state. This suggests electron capture into an excited state of the defect prior to decay to the ground configuration. Two possible mechanisms exist: (i) If reorientation is possible in the excited state, and its lifetime is long enough for thermal equilibrium to be established, subsequent decay to the ground state could produce the observed alignment; (ii) Alternatively, an undistorted excited state could have its matrix elements to the different distorted ground configurations altered by the stress. In this case, the transition probabilities for decay to the different orientations would be correspondingly altered, producing the alignment. The first mechanism would produce a Boltzmann distribution between the distortions resulting in a temperature dependence of the alignment. The second mechanism would be temperature independent.

In Fig. 5 we show the alignment observed versus temperature and stress. The lack of temperature dependence suggests the second model where the capture matrix elements to the ground configuration are altered by the stress.

Careful study of the relative intensities of the resolved spectral components indicates that only a limited reorientation of the defect is occurring. In terms of the labeling notation, the first letter remains unchanged but the second letter changes. In terms of the models in Fig. 4, the high elec-
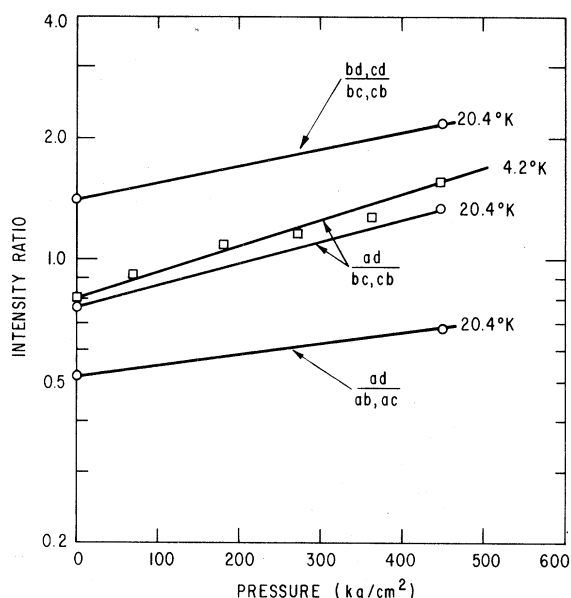

FIG. 5. Alignment produced by stress in the presence of light at the indicated temperatures, as measured by the ratios of the intensities of selected resolved multiplets.

tron density $\langle 111 \rangle$ axis associated with Q_3' remains fixed but the off-axis distortion of the boron can change between any of the three possible distortions.

The association of the alignment with the capture process and the failure to detect any alignment memory between bleaching and regeneration suggests that this off-axis distortion may occur only when the electron is captured.

B. Polarized light studies

Prolonged illumination with polarized light of energy near the band gap at 4.2 or 20.4 °K also is observed to produce an alignment in the spectrum. This is illustrated in Fig. 6. The nature of the alignment is qualitatively different from that described in Sec. IV A. Here the alignment is associated with a change in the *first* letter of the defect labeling scheme. In terms of the model of Fig. 4, the $\langle 111 \rangle$ axis associated with Q_3' has changed. The alignment is also of a much more permanent character. The alignment remains even after warming to $\gtrsim 180$ °K, recooling, and regenerating the spectrum with unpolarized light.

The dependence of the alignment upon the orientation of the polarization of the light is shown in Fig. 7. Plotted are the relative intensities of the different resolved spectral components after saturation alignment has occurred at each polarization direction. The maximum intensity of a specific defect orientation is seen to occur when the polarization vector is along the $\langle 111 \rangle$ Q_3' axis of
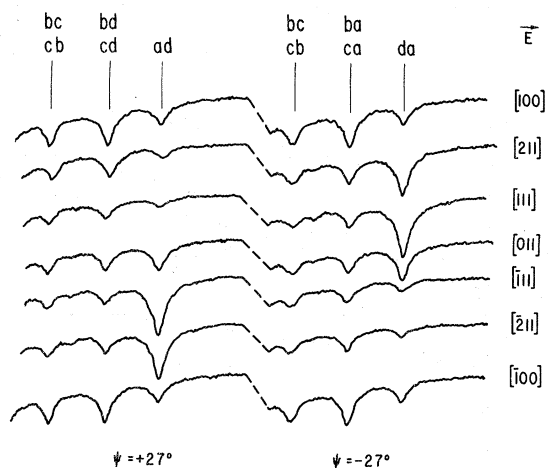
FIG. 6. Alignment achieved with polarized near-band-gap light at 20.4 °K, as seen in the intensities of the various spectral components, vs orientation of the polarization vector of the light. The resolved high-field spectral components at $\psi = \pm 27°$ are shown [Fig. 2(a)] and are labeled by their corresponding defect orientations.

the defect. The minimum intensity occurs when the polarization is perpendicular to this axis. This clearly demonstrates that the realignment is being stimulated by a local optical excitation at the defect. The sense of the alignment indicates that the optical transition has its dipole moment perpendicular to the high electron density $\langle 111 \rangle$ axis (Q_3') of the defect.

Such a process can be described as follows: The fraction of defects N_i oriented along the ith $\langle 111 \rangle$ axis is determined by the set of four simultaneous equations

$$N_i = -3W_{i \rightarrow j} N_i + \sum_{j \neq i} W_{j \rightarrow i} N_j . \qquad (8)$$

We take $W_{i \rightarrow j}$, the light-induced reorientation rate from the ith to the jth $\langle 111 \rangle$ orientation, as

$$W_{i \rightarrow j} = (1 - \cos^2 \theta_i) + K , \qquad (9)$$

where θ_i is the angle between $\vec{E}$ and the ith $\langle 111 \rangle$ axis. The factor K has been added to account for processes not reflecting the polarization of the light such as electron and hole capture at the defect, the nonpolarized component of the light, etc. In Fig. 7 the solid curves are values calculated from Eqs. (8) and (9) with $K = 0.9$. The agreement is good, confirming the interpretation.

The rate of the light-induced reorientation was studied as follows: A maximum alignment between the ad and da components (Fig. 6) was first produced with light polarized along the [111] direction. The EPR signal was then bleached with 10 000-Å light and the growth of the signals upon

regeneration with near-band-gap *unpolarized* light studied. The EPR signals initially emerge with full alignment. Upon prolonged illumination, the alignment decays exponentially as a result of the light-induced reorientation. With tungsten light passed through a water filter the time constant for reorientation was found to be ~1500 times that for generation.

A similar study was also performed to separate out the role of electron- and hole-capture processes at the defect in effecting its reorientation. Polarized light was again used to align the defects and the spectrum bleached with 10 000-Å light. The growth of the spectrum and the subsequent decay of the alignment was then studied versus 1.5-MeV electron dose to produce uniform ionization in the sample. Again it was found that the alignment decayed indicating ionization-induced reorientation. The reorientation rate was measured to be $\frac{1}{1200}$ that of the spectrum generation rate due to the ionization. From this we conclude that electron- or hole-capture processes are essentially as effective as direct optical excitation in reorienting the defect. This observation is consistent with the requirement of the constant K in Eq. (9).[21]

Thermally activated reorientation was studied by first optically aligning the defects, and then studying the isothermal decay of the alignment at
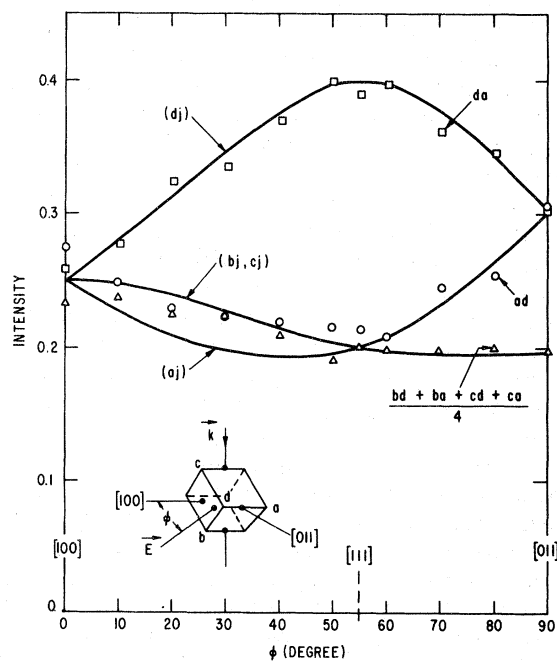

FIG. 7. Angular dependence of defect alignment produced by polarized light at 20.4 °K. The plotted points are the observed intensities of the indicated spectral components. The curve is a match to theory, see text.
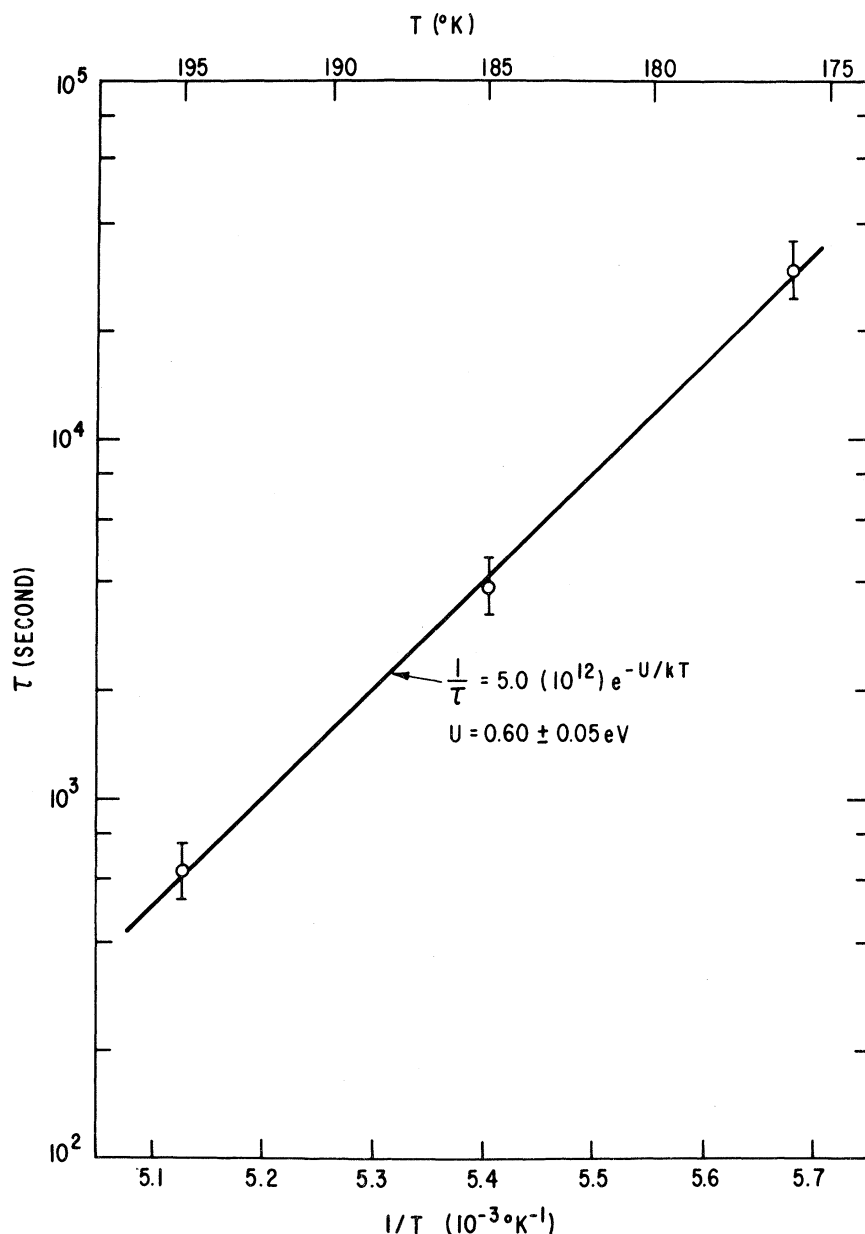
FIG. 8. Characteristic recovery time τ vs temperature for the alignment produced at 20.4 °K by polarized light.

$$\frac{1}{\tau} = 5.0 \ (10^{12}) \ e^{-U/kT}$$

$$U = 0.60 \pm 0.05 \, eV$$

various temperatures in the dark. After each anneal, the sample was cooled to 20.4 °K in the dark, the EPR signal regenerated with a short burst of light, and the alignment monitored. (Because of the large difference in light-induced realignment rates and generation rates, $\sim\frac{1}{1500}$, this monitoring procedure was possible without significantly altering the alignment.) Within accuracy the decay at each temperature appeared to be a simple exponential, characteristic of first-order kinetics. In Fig. 8 the characteristic reorientation time τ determined in these studies is given versus temperature. The thermal activation barrier for reorientation is thus determined to be

0.6 eV. The preexponential factor is a reasonable value for a local rearrangement process, being of the order of kT/h.

C. High-temperature stress studies

Uniaxial stress of ~ 500 kg/cm^2 was applied along the [0$\bar{1}$1] axis (see Fig. 3) of the crystal for 15 min at 220 °K and then the crystal was cooled to 20.4 °K with stress on. As can be seen from Fig. 8, thermally activated reorientation is fast enough at this temperature for equilibrium alignment to have been established. Upon regeneration of the signal with light at 20.4 °K, a small alignment was detected, the bj and cj orien-

tations having increased slightly over the aj, dj orientations (here j can be a, b, c, or d, but must be different from the first letter of the designation). The measured value was

$$(bj + cj)/(aj + dj) = 1.10 \pm 0.05 . \qquad (10)$$

Upon annealing for 15 min at 220 °K with stress off, the alignment disappeared.

The defect, therefore, prefers to align with its $\langle 111 \rangle$ Q_3' axis along the compressed direction.

The energy of a defect in an applied strain field can be written

$$E = \sum_{i,j} B_{ij} \epsilon_{ij} , \qquad (11)$$

where ϵ_{ij} are the strain tensor components and B_{ij} are the components of a symmetric second-rank "piezospectroscopic"[22] tensor $\overleftrightarrow{B}$. The number of independent components B_{ij} depends upon the symmetry of the defect. In Sec. IV A, one noted evidence that the off-axis distortion of the boron atom occurred only upon trapping an electron at low temperatures to give the EPR charge state (B°). In the B^+ charge state stable at the elevated temperatures where stress alignment is occurring, the center would, therefore, have trigonal symmetry, the $\langle 111 \rangle$ high electron density (Q_3') axis (first letter) being the trigonal axis. Kaplyanskii[22] has shown that for this symmetry the matrix $\overleftrightarrow{B}$ has only two independent parameters. In the trigonal axis system (the three axis is the high electron density axis of the defect) $\overleftrightarrow{B}$ has the form

$$\overleftrightarrow{B} = \begin{bmatrix} -B + B_0 & 0 & 0 \\ 0 & -B + B_0 & 0 \\ 0 & 0 & +2B + B_0 \end{bmatrix} . \qquad (12)$$

We equate the alignment in Eq. (10) to a Boltzmann distribution

$$n_b/n_a = \exp[-(E_b - E_a)/kT] , \qquad (13)$$

from which we determine $(E_b - E_a)$, where E_b and E_a are given by (11) for each defect orientation, and T is the temperature of the equilibrium alignment (~ 200 °K). For stress $\sigma(0\bar{1}1)$ along the $[0\bar{1}1]$ direction, Eqs. (11) and (12) lead to

$$B = (E_b - E_a)/S_{44}\sigma(0\bar{1}1) , \qquad (14)$$

where S_{44} is the shear elastic modulus of silicon ($= 12.56 \times 10^{-13}$ cm^2/dyn).[23] Our results give

$$B = +1.3 \text{ eV/(unit strain)}.$$

We cannot determine B_0, the coupling to the hydrostatic component of strain.

The above analysis also has significance even if an off-axis distortion of the defect remains

TABLE II. Activation energy for reorientation from one $\langle 111 \rangle$ bond axis to another (U) and average "trigonal" stress coupling coefficient (B) for interstitial boron, and other interstitial-related defects in silicon.

	B(int.)	C(int.) − C(sub.)	O(int.)
U (eV)	0.60 ± 0.06	1.21 ± 0.08[a]	2.561 ± 0.005[c]
B (eV)	$+1.3$	-6.4[b]	-7.6[d]

[a]K. L. Brower, Phys. Rev. B **9**, 2607 (1974).
[b]Estimated from Fig. 6 in Ref. a.
[c]J. W. Corbett, R. S. McDonald, and G. D. Watkins, J. Phys. Chem. Solids **25**, 873 (1964).
[d]Estimated from alignment values given in Ref. c.

under the conditions of stress. In that case, the observed alignment represents an average over the populations of the three off-axis distortions for each Q_3' $\langle 111 \rangle$ axis. As long as population changes are in the linear regime versus strain (i.e., $E \gtrsim kT$), this population average is fully equivalent to averaging the lower symmetry B tensor over these three distortions, which leads directly to the form of Eq. (12) for a trigonal center. In any event, this is the best that can be done with our data because no information is available concerning the stress coupling to the off-axis part of the distortion. Accordingly, we label B the average "trigonal" coupling coefficient in Table II. The low degree of alignment observed, Eq. (10), indicates that we should be in the linear regime.

V. ANNEALING STUDIES

A. Thermally activated annealing

An *isothermal* anneal was performed at 300 °K. In this study the sample was returned to 20.4 °K after each annealing period, the spectrum was regenerated with light, and the spectrum intensity monitored. Within experimental accuracy, the Si-G28 spectrum decay followed a simple exponential versus time

$$f(t) = e^{-t/\tau} , \qquad (15)$$

characteristic of first-order reaction kinetics. The time constant τ at 300 °K was measured to be 1700 sec.

In Fig. 9 we also show the results of *isochronal* anneals for two different annealing time intervals. (In these studies the 75-min annealing sequence was performed first. The same sample was then reirradiated and the 4-min annealing sequence performed.) Using Eq. (15) the time constant τ was estimated from the fractional recovery at each isochronal anneal in Fig. 9. The results are given in Fig. 10 along with the more accurate value estimated from the isothermal study at
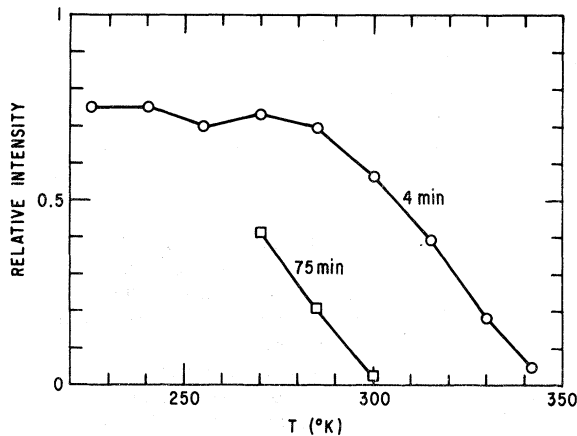
FIG. 9. Isochronal anneal of the Si-G28 spectrum for two annealing time intervals.

300 °K. Also shown in the figure is the straight line

$$\tau^{-1} = 5.3(10^6) \exp(-0.60 \text{ eV}/kT) ,$$

which represents an approximate match of the data to an activation energy of 0.6 eV.

The scatter of the points reveals the relative inaccuracy of the isochronal annealing studies. However, from Fig. 10 it is clear that the data are roughly consistent with an activation energy of ~0.6 eV.

In Sec. IV B, Fig. 8, the activation energy for reorientation of the major axis of the defect (Q_3') was measured to be 0.60 ± 0.05 eV. This suggests the possibility that the same limiting mechanism is involved in both anneal and reorientation. We note that if the model of Fig. 4(a) or Fig. 4(c) is correct, reorientation also causes the boron atom to move in the lattice. The activation energy for reorientation would also, therefore, be that for migration. Anneal could in turn result from diffusion of the boron to traps or sinks in the material. The preexponential factor found in the anneal, Fig. 10, is a factor of 10^6 smaller than that for reorientation, Fig. 8. This is fully consistent with the model of long-range diffusion, the factor of 10^6 representing ~10^6 single jumps before encountering a trap.

Other EPR spectra remain after the Si-G28 anneal. Most have not been analyzed. None appear to display resolved boron hyperfine interactions that would identify them as possible candidates for the trapped boron interstitial.

B. Athermal migration

In Sec. IV B it has been demonstrated that the defect can be made to reorient either by direct optical excitation on via electron- and hole-cap-

ture processes resulting from bulk ionization in the crystal. The fact that this process occurs even at 4.2 K suggests that the process is *athermal*, i.e., it does not require thermal activation to occur, the required energy being supplied directly from the electronic excitation. If migration accompanies reorientation, then this means that *athermal* defect migration[24] and annealing might be produced at low temperatures by this excitation.

To investigate this possibility the following experiment was performed: A sample was first irradiated with 1.5-MeV electrons at 20.4 °K to produce the Si-G28 spectrum. The sample was then illuminated for prolonged periods at 20.4 °K with approximately 0.24 W of 1.06-μm radiation from a YAlG: Nd laser. Under this illumination the time constant for reorientation was measured directly to be ~0.5 sec.

In Fig. 11 we plot the intensity of the Si-G28 spectrum versus accumulated time of 1.06-μm illumination, measured in units of the reorientation time at that illumination level. After an initial increase the intensity decays versus illumination time but eventually levels off. Also shown is the annealing curve predicted by the ratio of preexponential factors determined from the studies of thermally activated anneal and reorientation kinetics. This is the expected curve
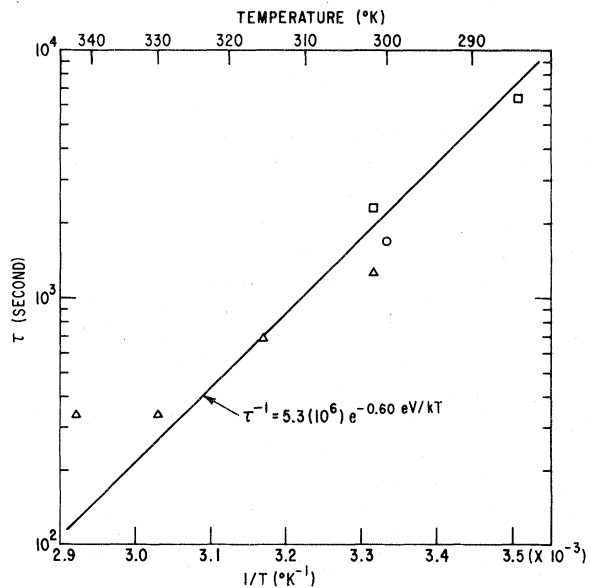

FIG. 10. Characteristic annealing time τ vs temperature. The circled point is from an isothermal anneal. The triangles (4 min) and squares (75 min) are calculated from the isochronal anneal studies of Fig. 9, assuming first-order reaction kinetics.
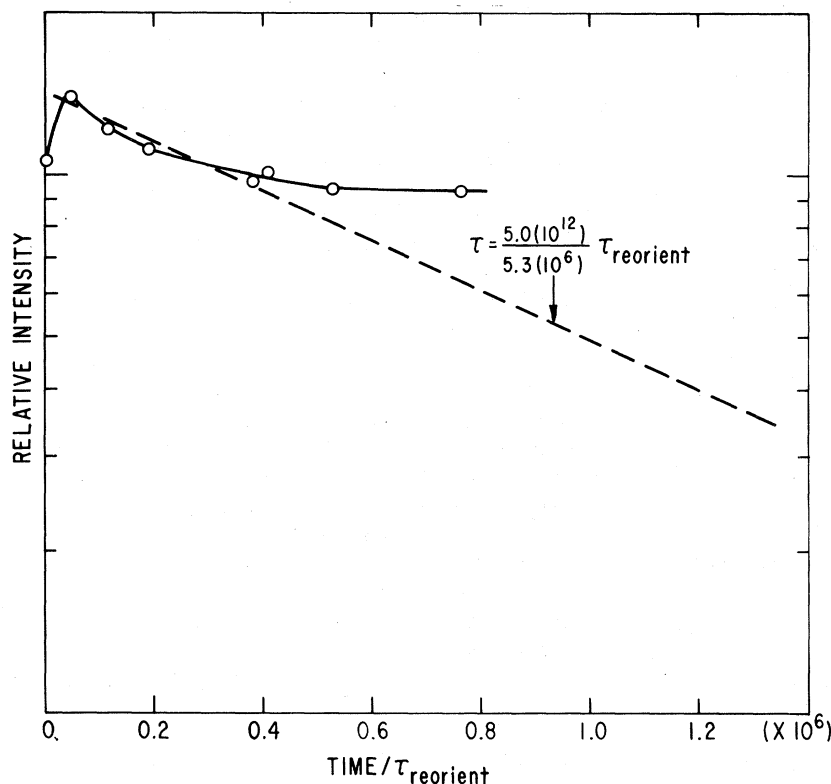
$$T = \frac{5.0(10^{12})}{5.3(10^6)} \, T_{reorient}$$

RELATIVE INTENSITY

0.   0.2   0.4   0.6   0.8   1.0   1.2   (X 10^6)

TIME/$T_{reorient}$

FIG. 11. Intensity of the Si-G28 spectrum vs time of illumination with 1.06-μm YAlG:Nd laser illumination at 20.4°K, The dashed curve is a prediction assuming that migration accompanies reorientation and that the identical annealing process is occurring at 20.4 and at 300°K.

if the identical annealing process is occurring.

During the initial decay other annealing processes are also observed to be occurring. Isolated vacancies, monitored by the Si-G1 spectrum, decrease in intensity and the Si-G10 spectrum, identified as a vacancy trapped by substitutional boron,[25] emerges. This, in turn, decays. This reveals the interesting result that vacancy migration is definitely being induced by the light as is the breakup of the boron-vacancy pairs. This, however, also clouds the interpretation of the initial Si-G28 decay which could be reflecting simply mobile vacancy-interstitial boron interactions. In addition the leveling off of the Si-G28 intensity-versus-illumination dose represents a clear departure from the predicted curve.

The results of Fig. 11 must be considered inconclusive. They do not provide direct evidence for migration of the interstitial boron. On the other hand, they cannot be interpreted to prove that migration is not occurring. The simple predicted decay curve of Fig. 11 assumes the identical annealing process at 20.4 °K and near 300 °K where the thermal annealing studies were performed. The possibility of different charge states for the traps and the diffusing boron interstitial at the two temperatures, temperature dependence of the capture cross sections, etc., all could destroy the equivalence.

VI. DISCUSSION

A. Electrical level structure

EPR is observed in the neutral charge state, consistent with $S = \frac{1}{2}$. The failure to see the resonance in the absence of light for both n- and p-type material reveals the presence of both a donor and acceptor level associated with the defect. If we interpret the loss of the Si-G28 resonance upon warming to ~50 °K in high resistivity p-type material as resulting from thermal excitation of the trapped electron from the donor state to the conduction band, its position can be estimated very approximately to be ~$E_c - 0.15$ eV.

B. Microscopic model

The anisotropy of the resonance reveals that neutral interstitial boron is not in one of the normal symmetrical tetrahedral (T_d) or hexagonal (D_{3d}) interstitial sites. Three possible models have been presented in Fig. 4.

In the model of Fig. 4(a) the boron is nestled between two normally bonded silicon atoms in a bent Si-B-Si interstitialcy configuration. This is similar to that established for interstitial oxygen in silicon. In Table II we compare the activation energy for reorientation from one ⟨111⟩ bond axis to another determined in this paper for boron with that previously measured for oxygen.[26] Also in-

cluded in the table is the stress coupling coefficient B, Eq. (12), determined for both.[27]

We have also included in the table the corresponding quantities estimated[27] for a carbon-carbon pair recently identified by Brower[28] in irradiated silicon. Brower's results can be interpreted to indicate that this center is a carbon-interstitial–carbon-substitutional pair. As such, it is presumably formed when a carbon interstitial, initially produced by the same replacement mechanism as that for interstitial aluminum and boron, migrates and is trapped by a second substitutional carbon atom. It bears many formal similarities to the interstitial boron spectrum studied here, also revealing a "bent" $\langle 111 \rangle$ structure.

The activation energy for $\langle 111 \rangle$ bond axis reorientation in Table II reveals a substantial decrease as one goes from oxygen to carbon to boron. This can be interpreted as evidence that the participation in the bonding, and the corresponding disruption of the normal silicon-silicon bonding, are progressively less as one moves to the left in the periodic table from oxygen to boron.

The strain coupling coefficient for both the oxygen and the carbon pair defects is large and of a sign consistent with the two substitutional atoms' being pushed apart and compressing the surrounding lattice correspondingly. The boron coupling is weak, however, and of the *opposite* sign. This observation must be considered a strong argument against the model of Fig. 4(a). It is difficult to see how the boron could nestle between the two silicon atoms and not produce a net compressive field along the defect axis.

The model of Fig. 4(c) is essentially that of a boron interstitial in the normal hexagonal interstitial site. In the neutral state, seen in EPR, it distorts out of this position owing to the Jahn-Teller effect. Here the negative charge density revealed by the Q_3' axis results from a filled nonbonding $2p$ orbital on the boron which is directed into the open interstitial spaces to either side of the hexagonal site. For this configuration the coupling to external strain might be expected to be weak. In fact, the observed sign of the coupling coefficient could reflect the dominance of the compressive stress against the six-membered puckered silicon ring in the plane perpendicular to the charge density Q_3' axis.

The model of Fig. 4(b) can be viewed as a distortion out of the tetrahedral interstitial site. Here, however, the distortion is one driven by a bonding force that remains for both B^+ and B^0. It is difficult to judge whether such a configuration, involving "back bonding" of a sort from Si(1), would occur or not. Here the EHT calculations on

diamond probably provide no insight because the silicon $3d$ unoccupied orbitals may well be important. Similarly, it is difficult to estimate the expected strain coupling coefficients.

The models of Figs. 4(a) and 4(c) have one important feature in common. For both, reorientation of the major Q_3' axis causes the defect to move in the lattice and is, therefore, equivalent to migration. This is not necessarily true for the model of Fig. 4(b). For it, reorientation could be confined to the cage surrounding a given tetrahedral site and migration would not necessarily occur.

The close correlation observed for the thermally activated reorientation kinetics and that for the disappearance of the interstitial boron upon anneal lends support to the idea that migration accompanies reorientation. However, the attempt to demonstrate this directly by observing annealing under photoexcitation at 20.4 °K was not successful. The question, therefore, of whether migration accompanies reorientation, and the corresponding implications concerning the various models, must be considered unresolved at this time.

C. Relationship to other studies

A number of experimental studies have been reported in the literature that relate to the properties of interstitial boron in silicon: North and Gibson[29] have observed a large fraction of boron in "nonsubstitutional" sites after boron implantation at room temperature. Using channeling techniques and the $^{11}B(p, \alpha)$ nuclear reaction, they were able to deduce that the boron atoms were not in the normal tetrahedral or hexagonal interstitial sites. Rather, they appeared to be located in line with the substitutional silicon atoms along $\langle 110 \rangle$ directions but not midway between two substitutional sites. We note that the model of Fig. 4(a) has many of these features. However, their center was observed to be stable to above 500 °C.

Bean *et al.*[30] have observed by infrared localized vibrational mode studies that room-temperature irradiation with 1.5–2.0-MeV electrons produces a decrease in substitutional boron and the growth of two new boron configurations. For one of these, labeled Q, two sharp localized vibrational bands were observed whose amplitudes reflect the isotropic abundance of ^{10}B and ^{11}B. This configuration was suggested to be isolated interstitial boron. The substitutional boron removal rate was high consistent with observed carrier removal rates, and a corresponding correlation with the growth of the Q bands was established. The Q bands disappear upon annealing at ~250 °C.

Both the ^{11}B(p, α) channeling technique and the infrared localized mode studies are highly specific to boron atoms, and their interpretation as revealing displaced boron atoms of some kind is, therefore, unambiguous. However, the high-temperature stability of the defects seen in these studies appears to be grossly inconsistent with our observations for the Si-G28 center, which is unstable at 300 °K. Three possibilities must be considered:

(i) The same defect configuration could be observed with the different stabilities resulting from differing charge states for the defect during anneal in each experiment. The studies reported in this paper were performed in p-type material, and the interstitial boron is presumed to be in the singly positive state during anneal. On the other hand, the channeling and infrared studies were performed on much more heavily damaged material, and the Fermi level position and resulting charge state for defects in these studies is not known. Charge-state effects have been observed in annealing studies of other defects in silicon (vacancy,[7,31] vacancy-phosphorus pair[32]). It is difficult, therefore, to rule this possibility out completely. However, the large activation energy change implied by a shift in the annealing from 300 to 525 to 775 °K makes this explanation unlikely.

(ii) The Si-G28 spectrum could result from a *metastable* configuration of the interstitial boron, and annealing simply result from conversion to a more stable isolated configuration which is the one observed in the other studies. [This would be consistent with the model of Fig. 4(b) where the reorientation studies in Sec. IV represents rattling around the interstitial cage and is in no way related to migration of the defect.] A strong argument against this interpretation is the annealing kinetics of Fig. 10. If annealing resulted from this simple one-jump conversion, the preexponential factor would be expected to be ~ 10^{13}, that of a characteristic vibrational frequency for the boron atom. A preexponential factor of ~ 10^7 is more characteristic of long-range motion, the atom making ~ 10^6 single jumps before being trapped.

(iii) The configurations observed in the infrared and channeling studies are not isolated interstitial boron at all, but interstitial boron in some kind of trapped configuration. This is, of couse, the most direct interpretation of the results, and is probably the correct one. Still, the fact that the infrared and channeling studies appear to reveal a single dominant configuration is somewhat surprising. Further experiments would be desirable to resolve these questions.

Another interesting recent experiment that has been interpreted in terms of boron interstitials is that of Tan et al.[33] They observed a series of sharp, well-resolved internal friction peaks in boron-implanted silicon, two of which they postulated were due to isolated interstitial boron in two different charge states. From the orientational dependence of the relaxation peaks, they deduced that the defect had orthorhombic $\langle 100 \rangle$ symmetry and postulated a $\langle 100 \rangle$ split-interstitial configuration for the boron. These identifications are clearly more speculative than the channeling and infrared studies. However, they indicate the potential power of this type of approach. Similar experiments in the future with low-temperature implants (where the Si-G28 spectrum is stable) could be highly informative. The particular peaks that these workers identified with interstitial boron annealed at ~ 300 °C. They displayed reorientation activation energies of 0.29 and 0.40 eV which seem to bear no relation to the 0.6 eV observed here for positively charged interstitial boron reorientation.

Interstitial boron has also been called upon as a model to describe defects observed in electrical studies of irradiated silicon. A donor level at ~ $E_V + 0.4$ eV has been observed in photoconductivity studies[34-36] and attributed by some[37,38] to interstitial boron. This defect is produced at room temperature as well as at cryogenic temperatures down to 4.2 °K and, from stress dichroism studies, was determined to have $\langle 111 \rangle$ C_{3v} symmetry.[36,38] It is stable to ~ 250 °C. In these experiments the Fermi level and charge state for interstitial boron should be similar to that in the studies reported in this paper. Therefore, we conclude that the identification of this photoconductivity level with isolated boron interstitials was not correct.

Several studies have shown an annealing recovery in the electrical properties of irradiated boron-doped p-type silicon at ~ 300–400 °K.[39-43] The kinetics for recovery in this region have variously been measured to have an activation energy from[42] 0.4 to[39] 0.7 to 1.1 eV.[41] It is likely that some or all of this annealing is to be associated with the instability of the isolated interstitial boron studied in this paper. However, in view of the scatter of these limited experimental results, a conclusive identification is not possible. (It is interesting to note that quenching studies in boron-doped silicon also produce defects that anneal at room temperature.[44,45] The annealing has been interpreted to indicate[44] 0.3 and[45] 0.8 eV for the activation energy of recovery.)

VII. SUMMARY

Isolated interstitial boron has been observed in its neutral charge state by EPR. It is produced

by 1.5-MeV electron irradiation at $\lesssim 20.4$ °K presumably when a mobile silicon interstitial atom produced in the primary damage event is trapped by substitutional boron. It appears to have three stable charge states ($+1$, 0, -1), serving as a donor in p-type material and acceptor in n type.

The Si-G28 spectrum reveals that the neutral boron atom is in neither the symmetrical tetrahedral (T_d) nor hexagonal (D_{3d}) interstitial site but is in a low-symmetry (C_{1h}) configuration. Several models have been suggested. For one, the boron is in an interstitialcy $\langle 111 \rangle$ Si-B-Si bonded configuration for both the positive and neutral charge state. An alternate model is a $\langle 111 \rangle$ Si-Si-B interstitialcy. In a third model the positively charged boron interstitial is in the hexagonal (D_{3d}) interstitial site, but distorts out of this site due to a Jahn-Teller distortion when it traps an electron to become B^0. The small coupling observed to uniaxial stress favors the third model.

The defect is unstable at room temperature, annealing over a period of ~ 30 min at 300 °K. The kinetics indicate an activation energy of ~ 0.6 eV and a preexponential factor consistent with long-range migration of a defect. An activation energy of 0.6 eV has also been found for thermally activated reorientation of the major $\langle 111 \rangle$ axis of the defect in a study at lower temperatures. This suggests that migration may accompany reorientation of the defect, a consequence of the first and third models.

Illumination with near-band-gap light at 4.2 or 20.4 °K can also induce this reorientation, as evidenced by alignment produced with polarized light. This suggests that *athermal* migration may be induced at these low temperatures by light. An attempt to demonstrate this by producing annealing at 20.4 °K with 1.06-μm light from a YAlG:Nd laser was not conclusive.

ACKNOWLEDGMENTS

*Present address: Dept. of Physics, Lehigh University, Bethlehem, Pa. 18015.

[1] G. D. Watkins, in *Radiation Damage in Semiconductors* (Dunod, Paris, 1965), p. 97.

[2] G. D. Watkins, in *Radiation Effects in Semiconductors*, edited by F. L. Vook (Plenum, New York, 1968), p. 67.

[3] G. D. Watkins, IEEE Trans. Nucl. Sci. NS-16, 13 (1969).

[4] K. L. Brower, Phys. Rev. B 1, 1908 (1970).

[5] G. D. Watkins and J. W. Corbett, Phys. Rev. 121, 1001 (1961).

[6] G. D. Watkins and J. W. Corbett, Phys. Rev. 134, A1359 (1964).

[7] G. D. Watkins, in Proceedings of the International Conference on Lattice Defects in Semiconductors, Freiburg, Germany 1974, (Institute of Physics, London, to be published).

[8] E. L. Elkin and G. D. Watkins, Phys. Rev. 174, 881 (1968).

[9] G. Wessel, Phys. Rev. 92, 1581 (1953).

[10] S. Fraga and G. Malli, University of Alberta Division of Theoretical Chemistry, Technical Report (unpublished).

[11] E. Clementi, IBM J. Res. Dev. Suppl. 9, 2 (1965).

[12] G. D. Watkins, Discuss. Faraday Soc. 31, 86 (1961).

[13] G. D. Watkins and J. W. Corbett, Phys. Rev. 138, A543 (1965).

[14] G. D. Watkins, Phys. Rev. 155, 802 (1967).

[15] T. P. Das and E. L. Hahn, *Nuclear Quadrupole Resonance Spectroscopy* (Academic, New York, 1958), p. 17.

[16] C. H. Townes and B. P. Dailey, J. Chem. Phys. 17, 782 (1949).

[17] H. J. Hrostowski and R. H. Kaiser, Phys. Rev. 107, 966 (1957).

[18] H. J. Hrostowski and B. J. Alder, J. Chem. Phys. 33, 980 (1960).

[19] D. R. Bosomworth, W. Hayes, A. R. L. Spray, and G. D. Watkins, Proc. R. Soc. Lond. A 317, 133 (1970).

[20] C. Weigel, D. Peak, J. W. Corbett, G. D. Watkins, and R. P. Messmer, Phys. Status Solidi B 63, 131 (1974).

[21] It is possible to achieve substantially greater alignment with polarized light than that of Fig. 7 if light greater than the band gap is selectively filtered out to reduce intrinsic electron-hole pair production. The results shown in Fig. 6 were produced with the addition of a Corning 7-69 filter for this purpose and display a maximum $da/\omega d$ alignment of 7.5:1.

[22] A. A. Kaplyanskii, Opt. Spektrosk. (Akad. Nauk SSSR Otd. Fiz.-Natl. Nauk.) 16, 602 (1964) [Opt. Spectrosc. 16, 329 (1964)].

[23] H. B. Huntington, in *Solid State Physics*, edited by F. Seitz and D. Turnbull (Academic, New York, 1958), Vol. 7, p. 274.

[24] The possibility of athermal migration in silicon has been discussed by R. E. McKeighen and J. S. Koehler, Phys. Rev. B 4, 462 (1971). See also a recent review by J. C. Bourgoin and J. W. Corbett, in *Lattice Defects in Semiconductors*, 1974 (Institute of Physics, London, 1975), p. 149.

[25] G. D. Watkins (unpublished).

[26] J. W. Corbett, R. S. McDonald, and G. D. Watkins, J. Phys. Chem. Solids 25, 873 (1964).

[27] We have estimated the average "trigonal" stress coupling coefficient B for the other centers in Table II using an analysis similar to that used for interstitial boron, Eqs. (12)–(14), from data available in the original references.

[28] K. L. Brower, Phys. Rev. B 9, 2607 (1974).

[29] J. C. North and W. M. Gibson, Appl. Phys. Lett. 16, 126 (1970).

[30] A. R. Bean, S. R. Morrison, R. C. Newman, and R. S. Smith, J. Phys. C 5, 379 (1972).

[31] B. L. Gregory, J. Appl. Phys. 36, 3765 (1965).

[32] L. C. Kimmerling, H. M. DeAngelis, and J. W. Diebold, Solid State Commun. 16, 171 (1975).

[33]S. I. Tan, B. S. Berry, and W. F. J. Frank, in *International Conference on Ion Implantation in Semiconductors and other Materials*, edited by B. L. Crowder (Plenum, New York, 1973), p. 19.

[34]V. S. Vavilov, A. F. Plotnikov, and V. D. Tkachev, Fiz. Tverd. Tela 4, 3446 (1962) [Sov. Phys.-Solid State 4, 2522 (1963)].

[35]A. H. Kalma and J. C. Corelli, Phys. Rev. 173, 734 (1968).

[36]L. J. Cheng, in *Radiation Effects in Semiconductors*, edited by F. L. Vook (Plenum, New York, 1968), p. 143.

[37]K. Matsui and P. Baruch, in *Lattice Defects in Semiconductors* (Pennsylvania State University, University Park, Pa., 1968), p. 282.

[38]M. Cherki and A. H. Kalma, Phys. Rev. B 1, 647

(1970).

[39]V. M. Malovetskaya, G. N. Galkin, and V. S. Vavilov, Fiz. Tverd. Tela 4, 1372 (1962) [Sov. Phys-Solid State 4, 1008 (1962)].

[40]H. J. Stein and R. Gereth, J. Appl. Phys. 39, 2890 (1968).

[41]L. L. Sivo and E. E. Klontz, Phys. Rev. 178, 1264 (1969).

[42]V. S. Vavilov, B. N. Mukashev, and A. V. Spitsyn, in *Defects in Semiconductors*, edited by J. Whitehouse (Institute of Physics, London, 1972), p. 284.

[43]J. W. Walker and C. T. Sah, Phys. Rev. B 7, 7 (1973).

[44]G. Bemski and C. A. Dias, J. Appl. Phys. 35, 2983 (1964).

[45]M. L. Swanson, Phys. Status Solidi 33, 721 (1969).